AGU ADVANCING EARTH AND SPACE SCIENCES

Geophysical Research Letters®

RESEARCH LETTER
10.1029/2023GL106365

# Increased Uncertainty in Projections of Precipitation and Evaporation Due To Wet-Get-Wetter/Dry-Get-Drier Biases

**Ori Adam[1], Maya Shourky Wolff[1], Chaim I. Garfinkel[1], and Michael P. Byrne[2]**

[1]Fredy and Nadine Herrmann Institute of Earth Sciences, Hebrew University, Jerusalem, Israel, [2]School of Earth and Environmental Sciences, University of St Andrews, St Andrews, UK

**Key Points:**

- Biases in the representation of the present hydroclimate lead to spurious but correctable projected changes in precipitation and evaporation
- A wet-get-wetter/dry-get-drier scaling bias adjustment can be applied separately to precipitation and evaporation
- The spurious changes increase uncertainty in precipitation and evaporation projections by up to 30% and 15% respectively

**Supporting Information:**

Supporting Information may be found in the online version of this article.

**Correspondence to:**

O. Adam,
ori.adam@mail.huji.ac.il

**Citation:**

Adam, O., Shourky Wolff, M., Garfinkel, C. I., & Byrne, M. P. (2023). Increased uncertainty in projections of precipitation and evaporation due to wet-get-wetter/dry-get-drier biases. *Geophysical Research Letters*, *50*, e2023GL106365. https://doi.org/10.1029/2023GL106365

Received 12 SEP 2023
Accepted 15 NOV 2023

**Author Contributions:**

**Conceptualization:** Ori Adam, Maya Shourky Wolff, Chaim I. Garfinkel
**Formal analysis:** Ori Adam, Maya Shourky Wolff
**Methodology:** Ori Adam, Maya Shourky Wolff
**Visualization:** Ori Adam
**Writing – original draft:** Ori Adam
**Writing – review & editing:** Chaim I. Garfinkel, Michael P. Byrne



**Abstract** A key implication of the well known wet-get-wetter/dry-get-drier (WGW) scaling is that model biases in the representation of precipitation and evaporation in the present climate lead to spurious projected changes under global warming. Here we estimate the extent of such spurious changes in projections by 60 models participating in phases 5 and 6 of the Coupled Model Intercomparison Project. Utilizing known thermodynamic constraints on evaporation, we show that the WGW scaling can be applied to precipitation and evaporation separately (specific WGW scaling), which we use to correct for spurious projected changes in precipitation and evaporation over tropical oceans. The spurious changes in precipitation can be of comparable amplitude to projected changes, but are generally small for evaporation. The spurious changes may increase the uncertainty in projections of tropical precipitation and evaporation by up to 30% and 15% respectively.

**Plain Language Summary** It is well established that if winds are assumed unchanged, the response of the hydrological cycle to global warming will follow the simple rule that wet regions get wetter and dry regions get drier. A key implication of this rule is that climate model errors in the representation of precipitation and evaporation in the present climate lead to artificial simulated responses in a warming climate. Here we show that this simple rule can be applied separately to precipitation and evaporation over tropical oceans. We then use this rule to estimate the extent of the artificial response over tropical oceans to global warming in modern climate models, caused by errors in the representation of precipitation and evaporation. Overall, the artificial changes may increase the uncertainty in projections by up to 30% for precipitation and 15% for evaporation.

## 1. Introduction

Changes in the hydrological cycle under global warming are commonly separated into two major contributions: (a) those resulting from changes in humidity (hereafter "thermodynamic"), and (b) those involving changes in the winds (hereafter "dynamic"; e.g., Emori & Brown, 2005; Ma et al., 2018; Seager et al., 2010; Wills et al., 2016). Over oceans, the thermodynamic changes are generally robust across models and well-captured by the "wet-get-wetter/dry-get-drier" scaling (WGW hereafter), which states that changes in precipitation minus evaporation ($P - E$) under global warming are proportional to $P - E$ in the present climate (Allan et al., 2020; Byrne & O'Gorman, 2015; Chou & Neelin, 2004; Held & Soden, 2006). Given the strong dependence of simulated thermodynamic changes on the representation of the present hydroclimate, the aim of this work is to assess the sensitivity of projected changes in the tropical hydrological cycle over ocean to systematic biases in $P$ and $E$ in modern climate models.

Figure 1 shows the tropical ensemble-mean biases and projected changes per 1 K of tropical warming in $P$ and $E$ by models participating in the fifth and sixth phases of the Coupled Model Intercomparison Project (CMIP5/6, see Section 2 for details; Eyring et al., 2016; K. E. Taylor et al., 2012). Large and robust changes and biases in $P$ and $E$ are seen in the tropics and are the focus of this study. Moreover, the tropical changes and biases overlap for both $P$ and $E$, in particular in the vicinity of the intertropical convergence zone (ITCZ), emphasizing the concern that biases in the present climate affect the projections.

The systematic tropical $P$ biases in the Pacific and Atlantic are generally known as the "double ITCZ bias", where modern climate models tend to overestimate $P$ south of the equator and underestimate $P$ along the equator (Adam et al., 2018; Fiedler et al., 2020; Lin, 2007; Mechoso et al., 1995). Along the equatorial Pacific, the underestimated $P$ is associated with a cold-tongue bias, which also inhibits $E$ there (e.g., Li et al., 2016). The underestimated evaporative cooling, in turn, may contribute to the warming seen along the equator in global warming projections

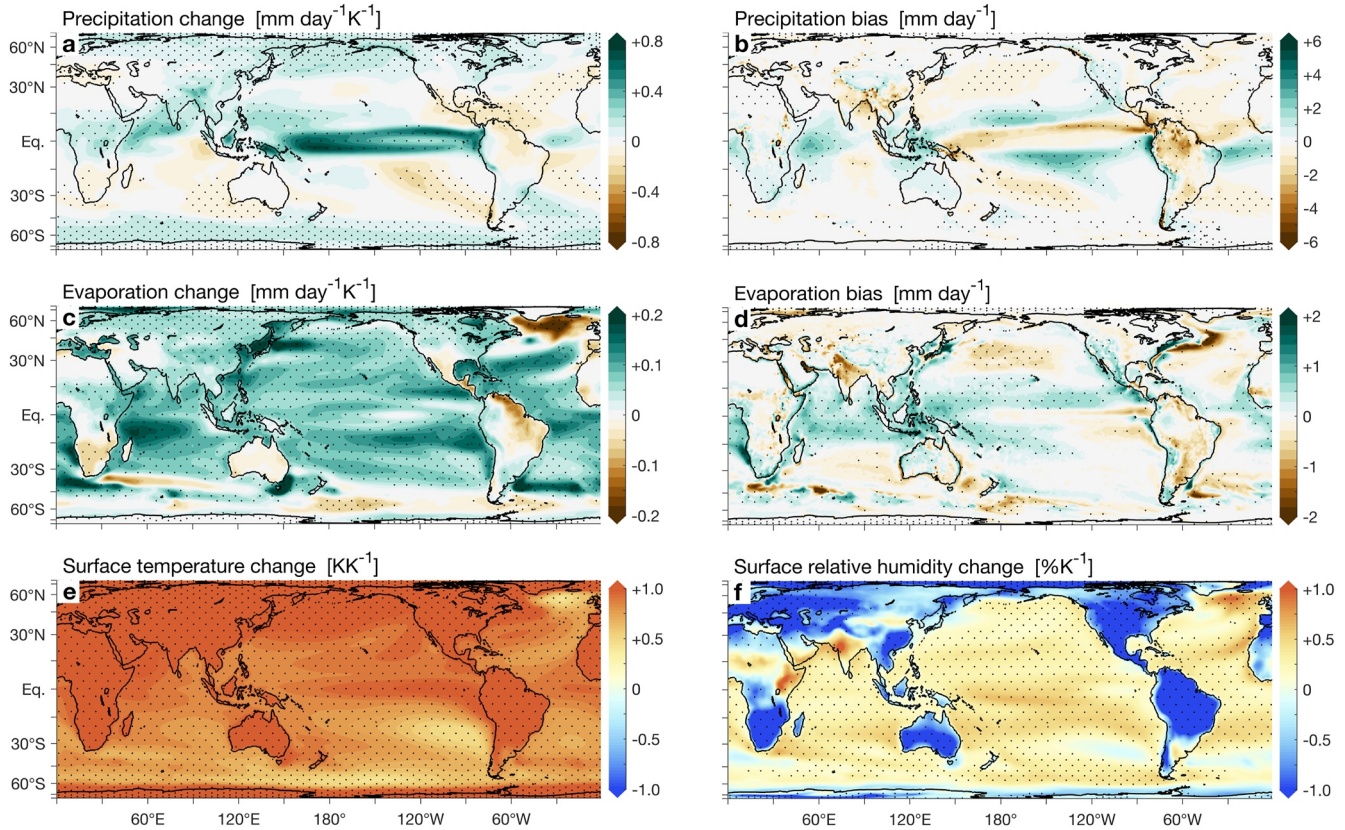


**Figure 1.** CMIP5/6 ensemble-mean sensitivity per 1 K tropical warming (change in mean surface air temperature equatorward of 30°) of (a) precipitation, (c) evaporation, (e) surface air temperature, and (f) surface relative humidity, and ensemble-mean biases in (b) precipitation, and (d) evaporation. The sensitivities to tropical warming are calculated using the difference between high-emission scenarios (RCP85/SSP585, 2080–2099) and historical simulations (1980–1999). The biases are calculated as the difference between historical simulations (1980–1999) and the European Center for Medium-Range Weather Forecasts ERA5 data set (1980–2020; Hersbach et al., 2020). Stippling indicates at least 80% of models agree on the sign of the bias or change. See Section 2 for details on the data and calculations.

(Figure 1e), in contrast to the observed strengthening of equatorial zonal sea surface temperature (SST) gradients in the Pacific (Coats & Karnauskas, 2017; Samanta et al., 2019; Seager et al., 2019). In the Asian and African sectors, *P* and *E* biases severely limit the reliability of monsoon-related predictions by CMIP5/6 models (e.g., M. A. Bollasina & Ming, 2013; M. Bollasina & Nigam, 2009; Prodhomme et al., 2014; Sperber et al., 2013). More generally, since deep convection occurs where surface temperatures exceed the tropical mean, tropical evaporation-related SST biases can strongly affect the projected *P* (also known as the "warmer-gets-wetter" mechanism; Chadwick et al., 2013; Huang et al., 2013; Johnson & Xie, 2010; Xie et al., 2010; Z.-Q. Zhou & Xie, 2015).

The complex nature of the climate system limits our ability to accurately quantify the direct effect of mean-state biases on projections. Moreover, while both the thermodynamic and dynamic components contribute to projected changes, the dynamic component dominates the uncertainty across models (Elbaum et al., 2022) and tends to counter thermodynamic changes over tropical oceans (Seager et al., 2010). This, in turn, makes it difficult to disentangle the effects of mean-state biases on thermodynamic and dynamic contributions. Nevertheless, previous works have found a strong influence of SST and *P* biases on projections of the tropical hydrological cycle, which can be largely traced to WGW (Dutheil et al., 2022; Lee et al., 2022; Li & Xie, 2014; Samanta et al., 2019; Z.-Q. Zhou & Xie, 2015; S. Zhou et al., 2020). The goal of the present analysis is to provide a simple framework for estimating the influence of *P* and *E* biases on projections of *P* and *E*. Specifically, we use known thermodynamic constraints on evaporation to separate the influences of *P* and *E* biases. The methods and theoretical framework are presented in Section 2, followed by our results and a discussion in Sections 3 and 4.

## 2. Data and Methods

### 2.1. Data

We analyze 40 climate models from phase 5 (K. E. Taylor et al., 2012) and 20 models from phase 6 (Eyring et al., 2016) of the Coupled Model Intercomparison Project (CMIP5/6). Calculations involving surface relative humidity and specific humidity at saturation were performed using subsets of 41 and 59 models, respectively, due to data availability (see Tables S1 and S2 in Supporting Information S1). For each model we use monthly data from the first realization (ensemble members "r1i1p1" and "r1i1p1f1" for CMIP5 and CMIP6, respectively), linearly interpolated to a common 1° × 1° horizontal grid. The CMIP5 and CMIP6 ensemble-mean climatologies analyzed here are nearly indistinguishable and are therefore presented jointly (hereafter CMIP5/6; Adam et al., 2022; Fiedler et al., 2020; Samuels et al., 2021; Tian & Dong, 2020). We focus our analysis on the annual mean, which, for the case of systematic tropical $P$ biases, is dominated by the January–June half year (Adam et al., 2018; Bellucci et al., 2010; Li & Xie, 2014). Seasonal plots of Figure 1 are provided in Figure S1 in Supporting Information S1. To account for the dependence of changes in $P$ and $E$ on the amplitude of tropical warming (Kent et al., 2015) we analyze their sensitivity per 1 K of tropical warming (changes in surface air temperature averaged equatorward of 30°), calculated as the difference between the end of century in high $CO_2$ emission scenarios (2080–2099 in the RCP85 and SSP585 scenarios of phases 5 and 6, respectively) and historical simulations (1980–1999), normalized by the change in tropical mean temperature for each model.

As reference data we use the European Center for Medium-Range Weather Forecasts (ECMWF) ERA5 reanalysis (0.25° × 0.25° resolution; Hersbach et al., 2020) during 1980–2020. Due to the scarcity of $E$ observations, a direct assessment of $E$ biases in the ERA5 reanalysis is not available. However, indirect estimates of combinations of $P$ and $E$ in ERA5 match direct observations as well as other reanalyzes, and also suggest ERA5 has a more physically consistent relation between $E$ and surface temperature than other modern reanalyzes (Vargas Godoy & Markonis, 2023). ERA5 generally tends to underestimate $P$ near the ITCZ and has an overall mean bias relative to in situ observations of about 0.2 mm day$^{-1}$. The CMIP5/6 $P$ bias relative to ERA5 exceeds 2 mm day$^{-1}$ in the regions of largest bias (Figure 1b) and is therefore not qualitatively sensitive to our choice of reference data (Hassler & Lauer, 2021; Samuels et al., 2021). We nevertheless repeat the analyses using $P$ from the Global Precipitation Climatology Project data set (GPCP, version 2.3; Adler et al., 2003) and $E$ from the Objectively Analyzed air-sea Fluxes data set (OAflux; Jin & Weller, 2008), but find no qualitative differences compared to the ERA5 results, with the exception that $E$ biases are significantly larger when the OAflux data set is used as reference.

### 2.2. WGW Bias Adjustment

The well-known WGW scaling (Held & Soden, 2006) is given by

$$\delta(P - E) = \alpha(P - E), \tag{1}$$

where the operator $\delta$ denotes the difference between the ends of the 21st and 20th centuries divided by the change in tropical mean temperature ($\Delta T$)

$$\delta \equiv \frac{(\cdot)_{21} - (\cdot)_{20}}{\Delta T} \tag{2}$$

and $\alpha = L/(R_v T^2)$ is the Clausius-Clapeyron (CC) parameter, where $L = 2.51 \times 10^6$ J kg$^{-1}$ is the latent heat of vaporization, $R_v = 461$ J kg$^{-1}$ K$^{-1}$ is the gas constant for water vapor, and $T$ is surface air temperature. The CC parameter is generally uniform in the tropics (Figure S2a in Supporting Information S1), and its CMIP5/6 tropical mean is $\alpha = 0.0615 \pm 0.5\%$ for fractional uncertainty of 1 standard deviation across models.

The assumptions of the WGW scaling are that:

1. Column-integrated water vapor scales with surface temperature at invariant relative humidity, and obeys the well-known CC scaling,

$$\delta q^* = \alpha q^* \tag{3}$$

where here $q^*$ denotes surface specific humidity at saturation;

2. Changes in surface temperature gradients are negligible; and
3. There are no changes in the winds.

As shown by Siler et al. (2019), mean thermodynamic changes in $E$ are given by

$$\delta E = \alpha^* E \tag{4a}$$

where

$$\alpha^* \equiv \left(1 + \frac{\alpha L q^*}{c_p}\right)^{-1} \left(\alpha - \frac{2}{T}\right) \tag{4b}$$

and where $c_p$ is the specific heat capacity of air at constant pressure (for convenience, the derivation of $\alpha^*$ is repeated in Supporting Information S1). Like $\alpha$, the parameter $\alpha^*$ is generally uniform in the tropics (Figure S2b in Supporting Information S1), with a tropical mean of $\alpha = 0.0140 \pm 3\%$ in CMIP5/6 models and negligible bias when compared with its ERA5 value (Figure S2c in Supporting Information S1).

Thermodynamic changes in $E$ are therefore smaller by a factor of about 4 than the changes expected from CC scaling, which is roughly the ratio of the amplitudes of tropical changes in $P$ and $E$ (Figures 1a and 1c). Combining Equations 1 and 4a yields for thermodynamic $P$ changes

$$\delta P = \alpha P - (\alpha - \alpha^*) E. \tag{5}$$

Equations 4a and 5 therefore provide a "specific WGW scaling," which can be applied to $P$ and $E$ separately. Interestingly, in regions where $E$ greatly exceeds $P$, such as the subtropics, this scaling predicts a negative precipitation response (Held & Soden, 2006; Siler et al., 2018), consistent with the changes seen in Figure 1a.

A key implication of the general and specific WGW scalings is that mean-state biases in $P$ and $E$ can lead to spurious projected changes. Given that these biases are known a priori, WGW scaling also offers a simple corrective adjustment for projections,

$$\delta(P - E)_{adj} = \delta(P - E) - \alpha(P - E)_{bias} \tag{6a}$$

for the general scaling, and

$$\delta P_{adj} = \delta P - \alpha P_{bias} + (\alpha - \alpha^*) E_{bias} \tag{6b}$$

$$\delta E_{adj} = \delta E - \alpha^* E_{bias} \tag{6c}$$

for the specific scaling, where the subscripts $(\cdot)_{adj}$ and $(\cdot)_{bias}$ denote the adjusted projection and present-day bias, respectively.

Thus, it may be possible to adjust for $P$ and $E$ biases that are directly translated to projected changes via WGW scaling.

### 2.3. Relation of the WGW Scaling to Thermodynamic and Dynamic Changes

Before analyzing the WGW bias adjustments we wish to provide context for the thermodynamic changes and clarify their relation to dynamic changes. We adopt the methodology described in Seager et al. (2010), which also includes a comprehensive derivation and analysis of the various components described below. Specifically, to first order, the sensitivity of $P - E$ to tropical warming can be decomposed into terms referred to here as thermodynamic (TH), dynamic (DYN), covariant (COV), and transient eddy,

$$\delta(P - E) \approx \delta\mathrm{TH} + \delta\mathrm{DYN} + \delta\mathrm{COV} + \delta\mathrm{TE} \tag{7a}$$

$$\delta\mathrm{TH} \equiv -\frac{1}{g\rho_w} \int_0^{p_s} \left[ \overbrace{(\bar{\mathbf{u}} \cdot \nabla \delta q)}^{\text{Advective}} + \overbrace{\delta q (\nabla \cdot \bar{\mathbf{u}})}^{\text{Divergent}} \right] \mathrm{d}p \tag{7b}$$

$$\delta\mathrm{DYN} \equiv -\frac{1}{g\rho_w}\int_0^{p_s} \nabla\cdot(\bar{q}\delta\mathbf{u})\mathrm{d}p \tag{7c}$$

$$\delta\mathrm{COV} \equiv -\frac{1}{g\rho_w}\int_0^{p_s} \nabla\cdot(\delta\mathbf{u}\delta q)\mathrm{d}p \tag{7d}$$

$$\delta\mathrm{TE} \equiv -\frac{1}{g\rho_w}\int_0^{p_s} \delta\left(\nabla\cdot\mathbf{u}'q'\right)\mathrm{d}p \tag{7e}$$

where $\overline{(\cdot)}$ and $(\cdot)'$ denote mean over the end of the 20th century and deviation thereof, and where $g = 9.81$ m s$^{-2}$ is the gravitational constant, $\rho_w = 10^3$ kg m$^{-3}$ is the density of water, $p$ is pressure, $\mathbf{u}$ is the horizontal wind field, and $q$ is specific humidity.

As demonstrated in Figure 2, the general WGW scaling is most closely linked to the divergent thermodynamic component ($\delta\mathrm{TH}_{\mathrm{div}}$; Boos, 2012; Seager et al., 2010, 2014). Specifically, since the WGW scaling assumes weak surface gradients and fixed winds, the advective thermodynamic component ($\delta\mathrm{TH}_{adv}$) and the dynamic component ($\delta$DYN) vanish under these assumptions. However, even for fixed winds, $\delta$TE does not vanish due to humidity changes that scale with CC. The WGW scaling therefore implicitly includes some of the contribution of transient eddies to moisture convergence (Held & Soden, 2006; Siler et al., 2023).

The key discrepancies between the WGW scaling and $\delta\mathrm{TH}_{\mathrm{div}}$ are that $P-E$ peaks are lower by about 20% and subtropical $P-E$ minima are weaker by up to 50%, especially in regions characterized by low level clouds (Zhang et al., 2023). Nevertheless, the ensemble-mean $\mathrm{TH}_{\mathrm{div}}$ and WGW scaling agree spatially very well (see Figure S3a in Supporting Information S1 for spatial correlations across models). Extensions of the WGW scaling that account for the effects of changes in surface temperature gradients (Boos, 2012) and relative humidity (Byrne & O'Gorman, 2015) provide second-order corrections (especially over ocean) which are therefore not considered here.

The dynamic component ($\delta$DYN Figure 2c) is generally larger than the thermodynamic component (or WGW, Figures 2a and 2b), but also generally negatively correlated with thermodynamic changes in the tropics (Figure S3b in Supporting Information S1), indicating competing contributions (Seager et al., 2010). Thus, counter to intuition, since the total change in $P-E$ is dominated by $\delta$DYN, the WGW scaling and total projected changes in $P-E$ are generally negatively correlated in the tropics (Figure S3c in Supporting Information S1). The $P$ and $E$ biases therefore introduce errors not only to projected $P$ and $E$ values, but also to the balance between dynamic and thermodynamic processes.

## 3. Results

We use the WGW bias adjustment (Equation 6) to assess the extent of the translated biases in projections of $P$ and $E$, and to subsequently provide an improved projection. To account for spatial variations in surface temperature, we use spatially varying $\alpha$ and $\alpha^*$ in Equation 6. The results however do not qualitatively differ if tropical mean values of these parameters are used.

### 3.1. Precipitation Bias Adjustment

The annually averaged adjusted projected $\delta P$ ($\delta P_{adj}$) and its WGW bias adjustment (Equation 6b) in the tropics are shown in Figures 3a and 3b (see Figure S4 in Supporting Information S1 for seasonal results). We highlight regions in the Western Equatorial Pacific, in the North Western tropical Pacific, and in the Southern tropical Pacific and Atlantic (rectangles in panels a and b) where $P$ biases are significant and large and where the WGW underlying assumptions are most valid (Figure 1b and Figure S3a in Supporting Information S1).

A negative $P$ bias is seen in the Western Equatorial Pacific region, associated with the equatorial Pacific cold-tongue bias (Note that disagreement across observational data sets is relatively high around the Pacific warm pool (Fiedler et al., 2020; Tian & Dong, 2020), increasing the uncertainty of our results in this region.) (Fiedler et al., 2020; Li & Xie, 2014; Tian & Dong, 2020). In the Eastern Pacific and Atlantic, excessive southward migration of the ITCZ during the southern hemisphere rainy season leads to overestimated $P$ south of the equator (Figures 1 and 3b; Adam et al., 2018; Li & Xie, 2014), which are reinforced by WGW in the projected

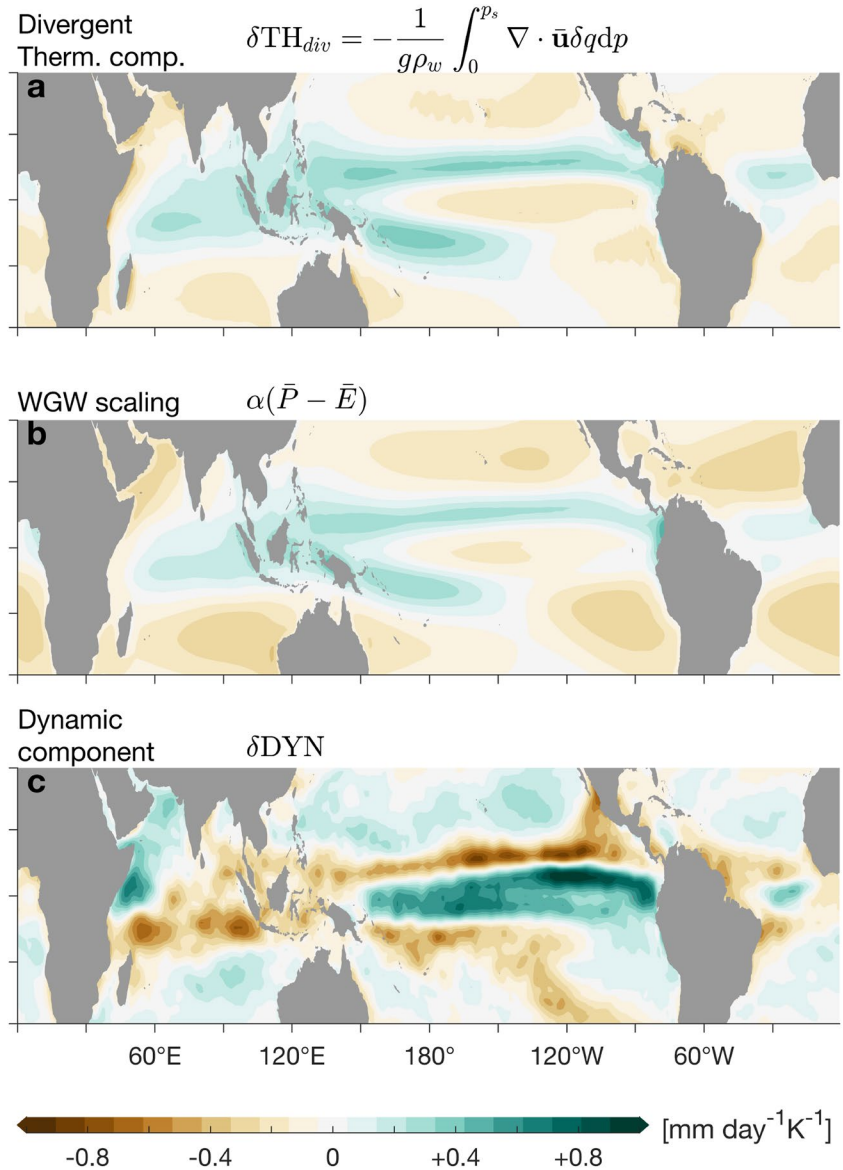


**Figure 2.** CMIP5/6 ensemble-mean annual-mean change per 1 K tropical warming in (a) the divergent thermodynamic component of changes in precipitation minus evaporation ($P - E$), (b) the wet-get-wetter (WGW) scaling, and (c) the dynamic component of changes in $P - E$.

climate. Indeed, the WGW adjustment increases the projected $P$ by about 20% in the Western Equatorial Pacific (Figure 3c) and is of comparable amplitude to $\delta P$ in the northern and southern regions (Figures 3d and 3e). In the Southern tropical Pacific and Atlantic, the adjusted $P$ shows significantly enhanced drying. Furthermore, Figure 3b suggests that the projected WGW biases lead to a spurious northward shift of the ITCZ in the Indian Ocean and a spurious southward shift of the Pacific ITCZ. These spurious meridional regional shifts are qualitatively similar to CMIP6 ensemble-mean projected shifts (Mamalakis et al., 2021), but do not exceed 1 degree at any longitude, and therefore only weakly affect the ensemble-mean shifts (Figure S5 in Supporting Information S1).

Given that $P_{bias}$ greatly exceeds $E_{bias}$ throughout most of the tropics, neglecting the contribution of $E$ biases yields nearly identical results to those presented in Figure 3 (Figure S6a in Supporting Information S1). These results do not qualitatively differ when the GPCP data set is used as reference (Figure S6b in Supporting Information S1). Similarly, the adjusted changes in $P$ are nearly indistinguishable from those of $P - E$, which are shown in Figure S7 in Supporting Information S1.

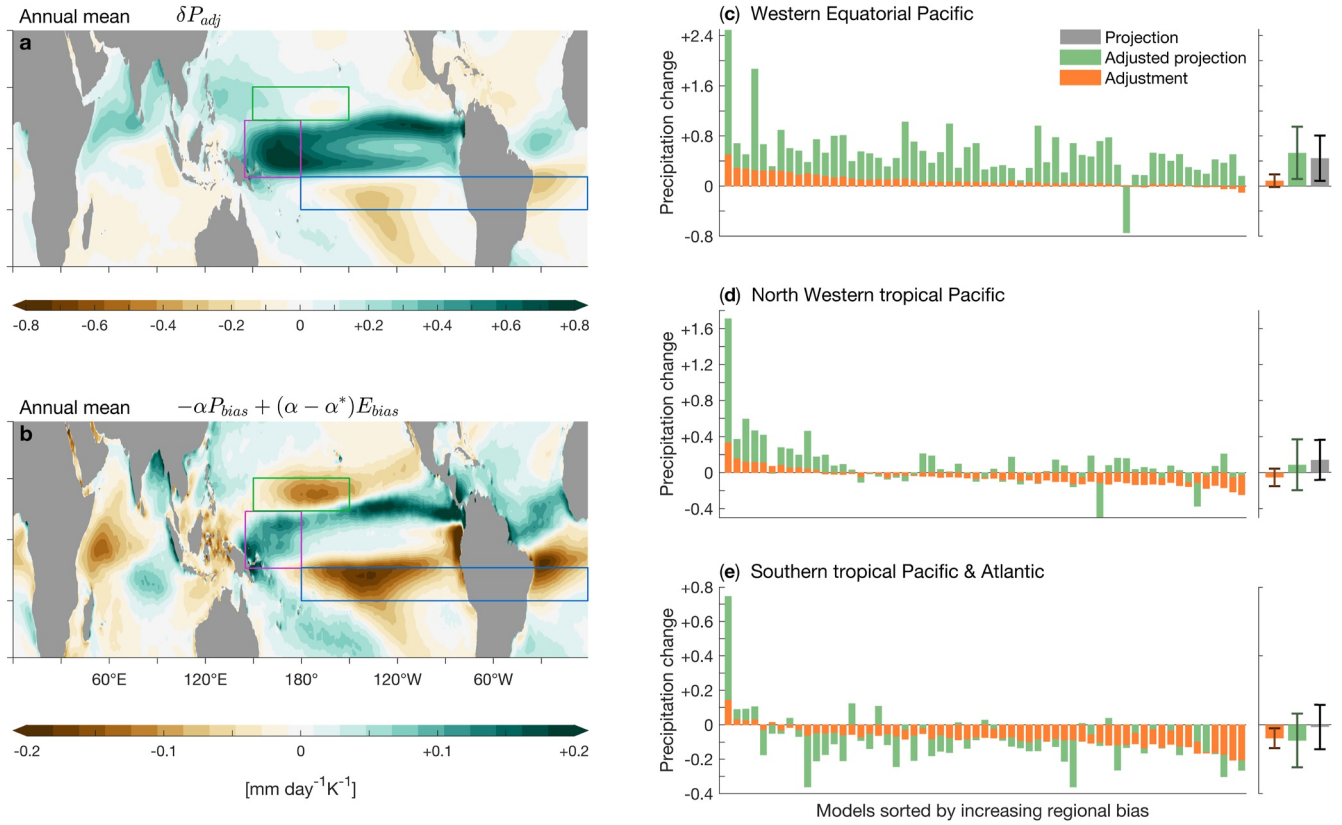


**Figure 3.** (a) Adjusted CMIP5/6 ensemble-mean projected change in precipitation per 1 K tropical warming. (b) CMIP5/6 ensemble-mean wet-get-wetter (WGW) bias adjustment per 1 K tropical warming. Mean values of the adjusted projection (green bars) and of the WGW adjustment (orange bars) in the (c) Western Equatorial Pacific (145°E–180°E, 7°S–7°N), (d) North Western tropical Pacific (150°E–210°E, 7°N–15°N), and (e) Southern tropical Pacific and Atlantic (180°E–360°E, 15°S–7°S), sorted by increasing regional bias (decreasing bias adjustment). Side bars in panels (c)–(e) show the ensemble-mean adjustment (orange), adjusted (green), and unadjusted (gray) projections. Error bars indicate uncertainty calculated as ±1 standard deviation across models.

Mean estimates of the hemispherically symmetric and anti-symmetric components of tropical systematic $P$ biases are commonly calculated using the equatorial precipitation index (EPI, Adam et al., 2016) and the precipitation asymmetry index (PAI, Hwang & Frierson, 2013), respectively,

$$\mathrm{EPI} = \frac{P_{[2°\mathrm{S}-2°\mathrm{N}]}}{P_{[20°\mathrm{S}-20°\mathrm{N}]}} - 1 \tag{8a}$$

$$\mathrm{PAI} = \frac{P_{[0-20°\mathrm{N}]} - P_{[20°\mathrm{S}-0]}}{P_{[20°\mathrm{S}-20°\mathrm{N}]}} \tag{8b}$$

where $P_{[\phi_1-\phi_2]}$ denotes the area-weighted zonal-mean $P$ between the latitudes $\phi_1$ and $\phi_2$.

**Table 1**
*Equatorial Precipitation Index (EPI) and Precipitation Asymmetry Index (PAI) Values for the ERA5 and GPCP Observational Data Sets, and for CMIP5/6 Historical Simulations, High-$CO_2$ Emission Scenarios (High-$CO_2$), and Adjusted Precipitation in High-$CO_2$ Emission Scenarios (High-$CO_{2,adj}$)*

| | ERA5 | GPCP | Historical | High-$CO_2$ | High-$CO_{2,adj}$ |
|---|---|---|---|---|---|
| EPI | 0.11 | 0.14 | 0.08 ± 0.11 | 0.18 ± 0.15 | 0.19 ± 0.12 |
| PAI | 0.19 | 0.20 | 0.04 ± 0.10 | 0.08 ± 0.09 | 0.11 ± 0.08 |

*Note.* Uncertainty is calculated as ±1 standard deviation across models.

The ERA5 EPI and PAI values are summarized in Table 1 and are 0.11 and 0.19, respectively, for the ERA5 data set (cf. Adam et al., 2016; Popp & Lutsko, 2017). The corresponding CMIP5/6 EPI values are within observed values in historical simulations and in the projections. PAI values however are significantly lower than observed in historical simulations; they increase in the projections, and increase further in the adjusted projections. Thus, the WGW adjustment has a weak effect on EPI but a strong effect on PAI (where the bias is more pronounced), bringing it closer to observed values.

10.1029/2023GL106365

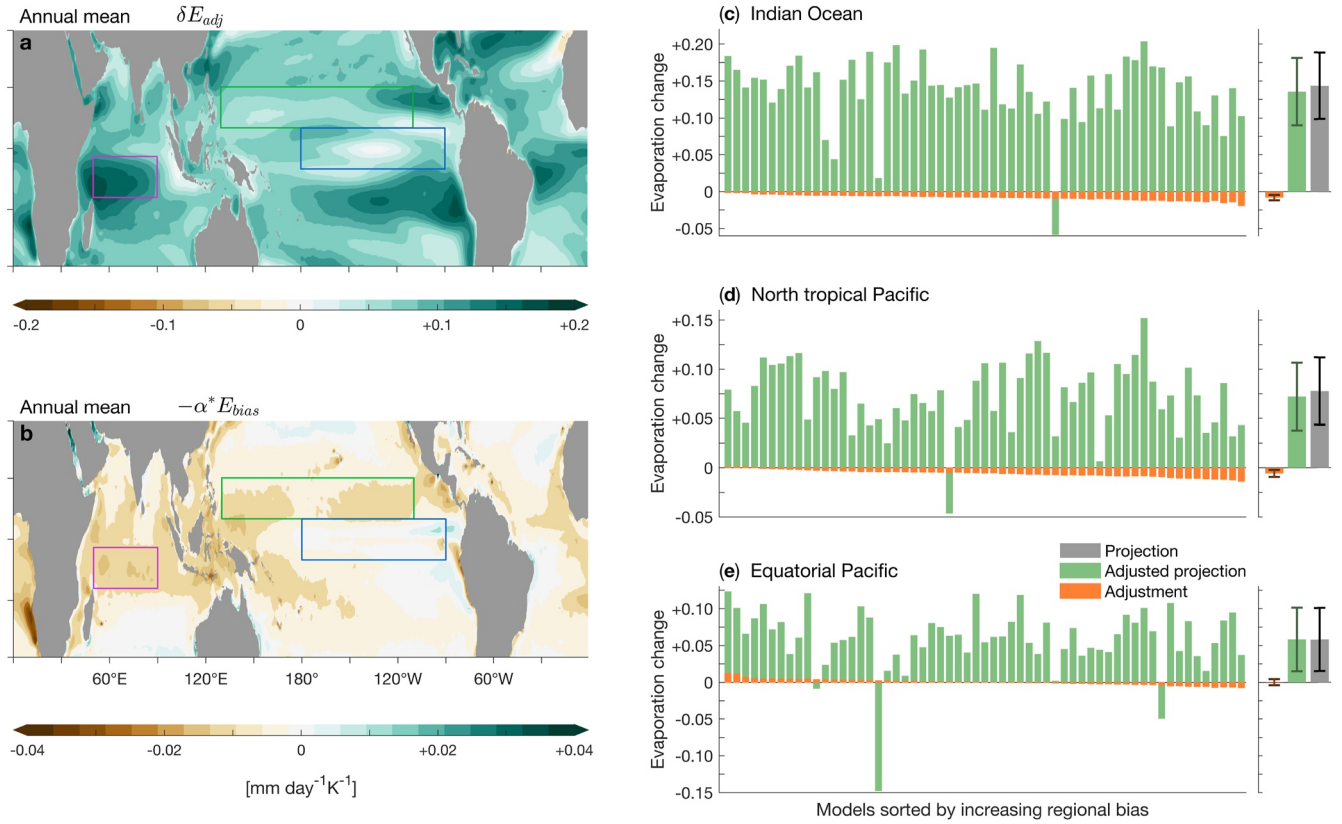


**Figure 4.** (a) Adjusted CMIP5/6 ensemble-mean projected change in evaporation per 1 K tropical warming. (b) CMIP5/6 ensemble mean wet-get-wetter (WGW) bias adjustment per 1 K tropical warming. Mean values of the adjusted projection (green bars) and of the WGW adjustment (orange bars) in the (c) Indian Ocean (50°E–90°E, 12°S–2°N), (d) North tropical Pacific (130°E–250°E, 5°N–15°N), and (e) Equatorial Pacific (180°E–270°E, 5°S–5°N), sorted by increasing regional bias (decreasing bias adjustment). Side bars in panels (c)–(e) show the ensemble-mean adjustment (orange), adjusted (green), and unadjusted (gray) projections. Error bars indicate uncertainty calculated as ±1 standard deviation across models.

### 3.2. Evaporation Bias Adjustment

The adjusted $E$ and the WGW bias adjustment for $E$ are shown in Figures 4a and 4b. First, we note that unlike the systematic $P$ biases, $E$ biases are positive throughout most of the tropics, and persist year round (Figures S1 and S8 in Supporting Information S1). The WGW adjustment therefore generally reduces $E$ in the tropics (i.e., it warms the tropics), except near the equatorial and southeastern tropical Pacific (Figure 4b).

We highlight regions in the Indian Ocean and in the northern and equatorial Pacific where $E$ changes and biases are significant (rectangles in Figures 4a and 4b). In the Indian Ocean and north Pacific regions (Figures 4c and 4d) the WGW adjustment reduces $E$ by about 10% (more so when the OAflux data is used as reference, as shown in Figure S9 in Supporting Information S1). In the equatorial Pacific, the mean WGW adjustment (Figure 4b) acts to increase $E$ in the Eastern Pacific relative to the Western Pacific, and therefore to increase the zonal SST gradient, but not consistently across models (Figure 4e). Overall, the WGW adjustment increases $E$ in the equatorial Pacific by 5% (10% when the OAflux data is used as reference). This weak effect suggests that thermodynamic effects alone cannot account for the spurious equatorial warming seen in CMIP5/6 projections, which has been associated with reduced evaporative cooling due to the Pacific cold-tongue bias (Samanta et al., 2019; Seager et al., 2019).

### 3.3. Adjusted Projection Uncertainty

The side panels of Figures 3c–3e and 4c–4e show the ensemble mean and uncertainty (±1 standard deviation across models) of the WGW adjustment (orange), adjusted projection (green), and unadjusted projection (gray). In the case where the projected change and the adjustment represent independent contributions to the total

uncertainty (i.e., the bias is independent of the projection), these uncertainties should be added in quadrature, that is, $\sigma_{Total} = \sigma\sqrt{1 + \sigma_{adj}^2/\sigma^2}$ where $\sigma_{total}$, $\sigma$, and $\sigma_{adj}$ denote the total uncertainty, uncertainty in projections, and uncertainty due to WGW biases (J. Taylor, 1997), representing a lower limit of the enhanced total uncertainty. However, where the bias adjustment is not independent of the change, uncertainty resulting from the WGW biases adds linearly to the total uncertainty, representing an upper limit of the total uncertainty, enhanced by mean-state biases.

The correlation between mean-state biases and projected change in $P$ and $E$ is generally weak but varies considerably throughout the tropics (Figure S10 in Supporting Information S1), suggesting that actual contribution by mean-state biases to the total uncertainty varies locally between the upper and lower limits. Specifically, averaged over tropical oceans, the uncertainty in the WGW adjustment is about 30% for $P$ and 15% for $E$ of the uncertainty in the unadjusted projected values, which agrees with the upper limit of uncertainty increase in specific regions. In the prescribed regions in Figure 3, uncertainty in the adjusted $P$ increases relative to projected values by 15%, 27%, and 20% in the Western Equatorial Pacific, North Western tropical Pacific, and Southern tropical Pacific and Atlantic, respectively. In the prescribed regions in Figure 4 the uncertainty in the adjusted $E$ increases relative to projected values by about 1% in all three regions but can reach 15% in parts of the subtropics (see Figure S11 in Supporting Information S1, showing the spatially varying increase in uncertainty in adjusted $P$ and $E$ relative to projected values).

Finally, the $P$ and $E$ biases influence the relative contribution of thermodynamic changes to the total projected changes. Specifically, the correlation of $\delta(P-E)$ with $\bar{P}-\bar{E}$ is negative throughout most of the tropics, and more so for $\delta(P-E)_{adj}$ (tropical mean correlations of $-0.27$ and $-0.35$, respectively, in Figure S3c and S3d in Supporting Information S1). Since WGW implies a positive correlation (as in Figure S3a in Supporting Information S1), this in turn suggests enhanced contrast between the dynamic and thermodynamic contributions, when mean-state biases are accounted for.

## 4. Summary and Discussion

The well known wet-get-wetter/dry-get-drier (WGW) scaling states that the thermodynamic response of precipitation minus evaporation ($P - E$) to global warming is proportional to the present hydroclimate (Held & Soden, 2006). Here we show that due to known thermodynamic constraints on $E$ (Siler et al., 2019), the WGW scaling can be applied to $P$ and $E$ separately (specific WGW scaling, Equations 5 and 4a). A key implication of the WGW scaling is that biases in the representation of $P$ and $E$ in the present climate are passed on to projected changes under global warming. Given that these biases are known a priori, we offer a correction based on the general and specific WGW scalings (Equation 6), which we assess in projections of the hydrological cycle over tropical oceans by 60 models participating in phases 5 and 6 of CMIP.

The spurious projected changes in $P$, caused by mean biases in historical simulations, lead to a 20% underestimate of the projected change in the Western Equatorial Pacific, a 50% overestimate in the North Western subtropical Pacific, and fail to capture an overall drying in the southern subtropical Pacific and Atlantic (Figure 3). Moreover, the projected biases introduce weak spurious regional shifts of the ITCZ (Figure S5 in Supporting Information S1).

The WGW scaling parameter for changes in $E$ is smaller by a factor of about 4 than the Clausius-Clapeyron scaling parameter (Siler et al., 2019), and therefore the spurious projected changes in $E$ are much smaller (generally less than 10%) than the projected changes (Figure 4). In particular, a weak negative bias adjustment in the equatorial Pacific suggests that thermodynamic evaporation biases alone cannot account for the spurious warming seen in the equatorial Pacific under global warming (Coats & Karnauskas, 2017; Samanta et al., 2019; Seager et al., 2019). However, given that $E$ biases are generally positive throughout the tropics, the WGW bias adjustment suggests excessive overall tropical cooling in CMIP5/6 projections.

While the WGW scaling and correction can be used to improve future projections, the improvement is limited by the assumptions that underlie WGW, and by the competing and interactive contributions of thermodynamic and dynamic processes to changes in $P - E$ (Seager et al., 2010). Specifically, the deviations of the projected $P - E$ from WGW are associated primarily with reduced $P$ along the margins of the $P$ climatology due to enhanced lateral moisture advection associated with $\delta \mathrm{TH}_{\mathrm{div}}$ (the "upped ante" mechanism; Chou & Neelin, 2004; Chou

et al., 2009; Neelin et al., 2003), spatial changes in tropical SST, especially on seasonal time scales (the "warmer gets wetter" mechanism; Huang et al., 2013; Z.-Q. Zhou & Xie, 2015), as well as changes in land-ocean temperature contrast and large-scale dynamics which affect surface winds (He & Soden, 2017). We therefore consider the adjusted projected $P$ and $E$ as a measure for estimating the potential influence of biases in $P$ and $E$ in lieu of a more accurate projection. Such corrections nevertheless may be applicable to specific regions where the WGW adjustment can be validated (cf. S. Zhou et al., 2020), and were shown in this paper to be potentially large.

Overall, we find that biases in the representation of the present hydroclimate can lead to notable spurious projected changes under tropical warming, which, due to the robustness of thermodynamic processes across models, influence the multi-model ensemble mean. Locally, mean-state biases may increase the projected uncertainty by up to ∼30% and ∼15% for $P$ and $E$, respectively.

## Data Availability Statement

All of the data used in the analyses presented here is publicly available. We thank the climate modeling groups for producing and making available their model output, the Earth System Grid Federation (ESGF) for archiving the data and providing access, and the multiple funding agencies who support CMIP and ESGF. All CMIP data analyzed here are available from the ESGF at https://esgf-node.llnl.gov/projects/esgf-llnl. The CMIP5 and CMIP6 models used here are listed in Tables S1 and S2 Supporting Information S1.

**Acknowledgments**
The research was supported by the Israel Science Foundation Grant 1022/21. We thank Nick Siler for sharing his insights on the thermodynamic evaporation response as well as an anonymous reviewer for helpful comments.

## References

Adam, O., Farnsworth, A., & Lunt, D. J. (2022). Modality of the tropical rain belt across models and simulated climates. *Journal of Climate*, *36*, 1331–1345. https://doi.org/10.1175/JCLI-D-22-0521.1

Adam, O., Schneider, T., & Brient, F. (2018). Regional and seasonal variations of the double-ITCZ bias in CMIP5 models. *Climate Dynamics*, *51*(1–2), 101–117. https://doi.org/10.1007/s00382-017-3909-1

Adam, O., Schneider, T., Brient, F., & Bischoff, T. (2016). Relation of the double-ITCZ bias to the atmospheric energy budget in climate models. *Geophysical Research Letters*, *43*(14), 7670–7677. https://doi.org/10.1002/2016gl069465

Adler, R. F., Huffman, G. J., Chang, A., Ferraro, R., Xie, P.-P., Janowiak, J., et al. (2003). The version-2 global precipitation climatology project (GPCP) monthly precipitation analysis (1979-present). *Journal of Hydrometeorology*, *4*(6), 1147–1167. https://doi.org/10.1175/1525-7541(2003)004<1147:tvgpcp>2.0.co;2

Allan, R. P., Barlow, M., Byrne, M. P., Cherchi, A., Douville, H., Fowler, H. J., et al. (2020). Advances in understanding large-scale responses of the water cycle to climate change. *Annals of the New York Academy of Sciences*, *1472*(1), 49–75. https://doi.org/10.1111/nyas.14337

Bellucci, A., Gualdi, S., & Navarra, A. (2010). The double-ITCZ syndrome in coupled general circulation models: The role of large-scale vertical circulation regimes. *Journal of Climate*, *23*(5), 1127–1145. https://doi.org/10.1175/2009jcli3002.1

Bollasina, M., & Nigam, S. (2009). Indian Ocean SST, evaporation, and precipitation during the South Asian summer monsoon in IPCC-AR4 coupled simulations. *Climate Dynamics*, *33*(7–8), 1017–1032. https://doi.org/10.1007/s00382-008-0477-4

Bollasina, M. A., & Ming, Y. (2013). The general circulation model precipitation bias over the southwestern equatorial Indian Ocean and its implications for simulating the South Asian monsoon. *Climate Dynamics*, *40*(3–4), 823–838. https://doi.org/10.1007/s00382-012-1347-7

Boos, W. R. (2012). Thermodynamic scaling of the hydrological cycle of the last glacial maximum. *Journal of Climate*, *25*(3), 992–1006. https://doi.org/10.1175/jcli-d-11-00010.1

Byrne, M. P., & O'Gorman, P. A. (2015). The response of precipitation minus evapotranspiration to climate warming: Why the "wet-get-wetter, dry-get-drier" scaling does not hold over land. *Journal of Climate*, *28*(20), 8078–8092. https://doi.org/10.1175/jcli-d-15-0369.1

Chadwick, R., Boutle, I., & Martin, G. (2013). Spatial patterns of precipitation change in CMIP5: Why the rich do not get richer in the tropics. *Journal of Climate*, *26*(11), 3803–3822. https://doi.org/10.1175/jcli-d-12-00543.1

Chou, C., & Neelin, J. D. (2004). Mechanisms of global warming impacts on regional tropical precipitation. *Journal of Climate*, *17*(13), 2688–2701. https://doi.org/10.1175/1520-0442(2004)017<2688:mogwio>2.0.co;2

Chou, C., Neelin, J. D., Chen, C.-A., & Tu, J.-Y. (2009). Evaluating the "rich-get-richer" mechanism in tropical precipitation change under global warming. *Journal of Climate*, *22*(8), 1982–2005. https://doi.org/10.1175/2008jcli2471.1

Coats, S., & Karnauskas, K. (2017). Are simulated and observed twentieth century tropical pacific sea surface temperature trends significant relative to internal variability? *Geophysical Research Letters*, *44*(19), 9928–9937. https://doi.org/10.1002/2017gl074622

Dutheil, C., Lengaigne, M., Vialard, J., Jullien, S., & Menkès, C. (2022). Western and central tropical pacific rainfall response to climate change: Sensitivity to projected sea surface temperature patterns. *Journal of Climate*, *35*(18), 6175–6189. https://doi.org/10.1175/jcli-d-22-0062.1

Elbaum, E., Garfinkel, C. I., Adam, O., Morin, E., Rostkier-Edelstein, D., & Dayan, U. (2022). Uncertainty in projected changes in precipitation minus evaporation: Dominant role of dynamic circulation changes and weak role for thermodynamic changes. *Geophysical Research Letters*, *49*(12), e2022GL097725. https://doi.org/10.1029/2022gl097725

Emori, S., & Brown, S. (2005). Dynamic and thermodynamic changes in mean and extreme precipitation under changed climate. *Geophysical Research Letters*, *32*(17), L17706. https://doi.org/10.1029/2005gl023272

Eyring, V., Bony, S., Meehl, G. A., Senior, C. A., Stevens, B., Stouffer, R. J., & Taylor, K. E. (2016). Overview of the coupled model intercomparison project phase 6 (CMIP6) experimental design and organization. *Geoscientific Model Development*, *9*(5), 1937–1958. https://doi.org/10.5194/gmd-9-1937-2016

Fiedler, S., Crueger, T., D'Agostino, R., Peters, K., Becker, T., Leutwyler, D., et al. (2020). Simulated tropical precipitation assessed across three major phases of the coupled model intercomparison project (CMIP). *Monthly Weather Review*, *148*(9), 3653–3680. https://doi.org/10.1175/mwr-d-19-0404.1

Hassler, B., & Lauer, A. (2021). Comparison of reanalysis and observational precipitation datasets including ERA5 and WFDE5. *Atmosphere*, *12*(11), 1462. https://doi.org/10.3390/atmos12111462

He, J., & Soden, B. J. (2017). A re-examination of the projected subtropical precipitation decline. *Nature Climate Change*, *7*(1), 53–57. https://doi.org/10.1038/nclimate3157

Held, I. M., & Soden, B. J. (2006). Robust responses of the hydrological cycle to global warming. *Journal of Climate*, *19*(21), 5686–5699. https://doi.org/10.1175/jcli3990.1

Hersbach, H., Bell, B., Berrisford, P., Hirahara, S., Horányi, A., Muñoz-Sabater, J., et al. (2020). The ERA5 global reanalysis. *Quarterly Journal of the Royal Meteorological Society*, *146*(730), 1999–2049. https://doi.org/10.1002/qj.3803

Huang, P., Xie, S.-P., Hu, K., Huang, G., & Huang, R. (2013). Patterns of the seasonal response of tropical rainfall to global warming. *Nature Geoscience*, *6*(5), 357–361. https://doi.org/10.1038/ngeo1792

Hwang, Y.-T., & Frierson, D. M. (2013). Link between the double-intertropical convergence zone problem and cloud biases over the Southern Ocean. *Proceedings of the National Academy of Sciences*, *110*(13), 4935–4940. https://doi.org/10.1073/pnas.1213302110

Jin, X., & Weller, R. A. (2008). Multidecade global flux datasets from the objectively analyzed air-sea fluxes (oaflux) project: Latent and sensible heat fluxes, ocean evaporation, and related surface meteorological variables. In *OAFlux project technical report OA-2008-01* (p. 74).

Johnson, N. C., & Xie, S.-P. (2010). Changes in the sea surface temperature threshold for tropical convection. *Nature Geoscience*, *3*(12), 842–845. https://doi.org/10.1038/ngeo1008

Kent, C., Chadwick, R., & Rowell, D. P. (2015). Understanding uncertainties in future projections of seasonal tropical precipitation. *Journal of Climate*, *28*(11), 4390–4413. https://doi.org/10.1175/jcli-d-14-00613.1

Lee, J., Kang, S. M., Kim, H., & Xiang, B. (2022). Disentangling the effect of regional SST bias on the double-ITCZ problem. *Climate Dynamics*, *58*(11–12), 3441–3453. https://doi.org/10.1007/s00382-021-06107-x

Li, G., & Xie, S.-P. (2014). Tropical biases in CMIP5 multimodel ensemble: The excessive equatorial Pacific cold tongue and double ITCZ problems. *Journal of Climate*, *27*(4), 1765–1780. https://doi.org/10.1175/jcli-d-13-00337.1

Li, G., Xie, S.-P., Du, Y., & Luo, Y. (2016). Effects of excessive equatorial cold tongue bias on the projections of tropical pacific climate change. Part I: The warming pattern in CMIP5 multi-model ensemble. *Climate Dynamics*, *47*(12), 3817–3831. https://doi.org/10.1007/s00382-016-3043-5

Lin, J.-L. (2007). The double-ITCZ problem in IPCC AR4 coupled GCMs: Ocean–atmosphere feedback analysis. *Journal of Climate*, *20*(18), 4497–4525. https://doi.org/10.1175/jcli4272.1

Ma, J., Chadwick, R., Seo, K.-H., Dong, C., Huang, G., Foltz, G. R., & Jiang, J. H. (2018). Responses of the tropical atmospheric circulation to climate change and connection to the hydrological cycle. *Annual Review of Earth and Planetary Sciences*, *46*(1), 549–580. https://doi.org/10.1146/annurev-earth-082517-010102

Mamalakis, A., Randerson, J. T., Yu, J.-Y., Pritchard, M. S., Magnusdottir, G., Smyth, P., et al. (2021). Zonally contrasting shifts of the tropical rain belt in response to climate change. *Nature Climate Change*, *11*(2), 143–151. https://doi.org/10.1038/s41558-020-00963-x

Mechoso, C. R., Robertson, A. W., Barth, N., Davey, M., Delecluse, P., Gent, P., et al. (1995). The seasonal cycle over the tropical pacific in coupled ocean–atmosphere general circulation models. *Monthly Weather Review*, *123*(9), 2825–2838. https://doi.org/10.1175/1520-0493(1995)123<2825:tscott>2.0.co;2

Neelin, J., Chou, C., & Su, H. (2003). Tropical drought regions in global warming and El Niño teleconnections. *Geophysical Research Letters*, *30*(24), 2275. https://doi.org/10.1029/2003gl018625

Popp, M., & Lutsko, N. (2017). Quantifying the zonal-mean structure of tropical precipitation. *Geophysical Research Letters*, *44*(18), 9470–9478. https://doi.org/10.1002/2017gl075235

Prodhomme, C., Terray, P., Masson, S., Izumo, T., Tozuka, T., & Yamagata, T. (2014). Impacts of Indian Ocean SST biases on the Indian Monsoon: As simulated in a global coupled model. *Climate Dynamics*, *42*(1–2), 271–290. https://doi.org/10.1007/s00382-013-1671-6

Samanta, D., Karnauskas, K. B., & Goodkin, N. F. (2019). Tropical Pacific SST and ITCZ biases in climate models: Double trouble for future rainfall projections? *Geophysical Research Letters*, *46*(4), 2242–2252. https://doi.org/10.1029/2018gl081363

Samuels, M., Adam, O., & Gildor, H. (2021). A shallow thermocline bias in the southern tropical pacific in CMIP5/6 models linked to double-ITCZ bias. *Geophysical Research Letters*, *48*(15), e2021GL093818. https://doi.org/10.1029/2021gl093818

Seager, R., Cane, M., Henderson, N., Lee, D.-E., Abernathey, R., & Zhang, H. (2019). Strengthening tropical Pacific zonal sea surface temperature gradient consistent with rising greenhouse gases. *Nature Climate Change*, *9*(7), 517–522. https://doi.org/10.1038/s41558-019-0505-x

Seager, R., Liu, H., Henderson, N., Simpson, I., Kelley, C., Shaw, T., et al. (2014). Causes of increasing aridification of the mediterranean region in response to rising greenhouse gases. *Journal of Climate*, *27*(12), 4655–4676. https://doi.org/10.1175/jcli-d-13-00446.1

Seager, R., Naik, N., & Vecchi, G. A. (2010). Thermodynamic and dynamic mechanisms for large-scale changes in the hydrological cycle in response to global warming. *Journal of Climate*, *23*(17), 4651–4668. https://doi.org/10.1175/2010jcli3655.1

Siler, N., Bonan, D. B., & Donohoe, A. (2023). Diagnosing mechanisms of hydrologic change under global warming in the CESM1 large ensemble. *Journal of Climate*, *36*(23), 8243–8257. https://doi.org/10.1175/jcli-d-23-0086.1

Siler, N., Roe, G. H., & Armour, K. C. (2018). Insights into the zonal-mean response of the hydrologic cycle to global warming from a diffusive energy balance model. *Journal of Climate*, *31*(18), 7481–7493. https://doi.org/10.1175/jcli-d-18-0081.1

Siler, N., Roe, G. H., Armour, K. C., & Feldl, N. (2019). Revisiting the surface-energy-flux perspective on the sensitivity of global precipitation to climate change. *Climate Dynamics*, *52*(7–8), 3983–3995. https://doi.org/10.1007/s00382-018-4359-0

Sperber, K., Annamalai, H., Kang, I.-S., Kitoh, A., Moise, A., Turner, A., et al. (2013). The Asian summer monsoon: An intercomparison of CMIP5 vs. CMIP3 simulations of the late 20th century. *Climate Dynamics*, *41*(9–10), 2711–2744. https://doi.org/10.1007/s00382-012-1607-6

Taylor, J. (1997). Introduction to error analysis, the study of uncertainties in physical measurements.

Taylor, K. E., Stouffer, R. J., & Meehl, G. A. (2012). An overview of CMIP5 and the experiment design. *Bulletin of the American Meteorological Society*, *93*(4), 485–498. https://doi.org/10.1175/bams-d-11-00094.1

Tian, B., & Dong, X. (2020). The double-ITCZ bias in CMIP3, CMIP5, and CMIP6 models based on annual mean precipitation. *Geophysical Research Letters*, *47*(8), e2020GL087232. https://doi.org/10.1029/2020gl087232

Vargas Godoy, M. R., & Markonis, Y. (2023). Water cycle changes in reanalyses: A complementary framework. *Scientific Reports*, *13*(1), 4795. https://doi.org/10.1038/s41598-023-31873-5

Wills, R. C., Byrne, M. P., & Schneider, T. (2016). Thermodynamic and dynamic controls on changes in the zonally anomalous hydrological cycle. *Geophysical Research Letters*, *43*(9), 4640–4649. https://doi.org/10.1002/2016gl068418

Xie, S.-P., Deser, C., Vecchi, G. A., Ma, J., Teng, H., & Wittenberg, A. T. (2010). Global warming pattern formation: Sea surface temperature and rainfall. *Journal of Climate*, *23*(4), 966–986. https://doi.org/10.1175/2009jcli3329.1

Zhang, Q., Liu, B., Li, S., & Zhou, T. (2023). Understanding models' global sea surface temperature bias in mean state: From CMIP5 to CMIP6. *Geophysical Research Letters*, *50*(4), e2022GL100888. https://doi.org/10.1029/2022gl100888

Zhou, S., Huang, G., & Huang, P. (2020). A bias-corrected projection for the changes in East Asian summer monsoon rainfall under global warming. *Climate Dynamics*, *54*(1–2), 1–16. https://doi.org/10.1007/s00382-019-04980-1

Zhou, Z.-Q., & Xie, S.-P. (2015). Effects of climatological model biases on the projection of tropical climate change. *Journal of Climate*, *28*(24), 9909–9917. https://doi.org/10.1175/jcli-d-15-0243.1